

A.J. Beer, O. Ratib, I. Dregely, M. Eiber, M. Essler,  
S. Foerster, S. Nekolla, C. Rischpler, J.-P. Willi,  
and I. Yakushev

## Contents

Benign, Degenerative and Inflammatory Diseases.....	211
Atherosclerotic Plaque at Carotid Bifurcation.....	212
Stress Fracture .....	214
Multicystic Disease.....	216
Kaposi Sarcoma.....	218
Maffucci Syndrome.....	220
Giant Cell Vasculitis.....	222
Cardiac Sarcoidosis.....	224
Frontotemporal Dementia (FTD).....	226
Alzheimer's Disease (AD).....	228
Posterior Cortical Atrophy.....	230
References .....	232

## Benign, Degenerative and Inflammatory Diseases

<sup>18</sup>F-FDG PET studies were shown to be quite sensitive to inflammation as well to a variety of benign diseases that induce focal increase in metabolism [1–3]. While in most countries PET imaging of these diseases are not reimbursed, it remains a potential alternative imaging modality for selected cases. FDG-PET remains a sensitive diagnostic modality for detection of infectious diseases and exploring sources of fever of unknown origin. In this chapter several diseases are presented, but also examples of identification and characterization of vascular plaques [4]. While <sup>18</sup>F-FDG is being reported as a potential marker of plaque inflammatory process and therefore may help identify unstable plaques and be a predictor of cardiovascular events, alternative PET tracers are also being evaluated for better characterization of vascular plaques [4–6].

Another application domain of PET and therefore could potentially benefit from hybrid PET/MR is the assessment of neurodegenerative diseases and differentiation of diagnostic classification based on anatomical distribution of brain metabolic activity. Many studies reported the added value of <sup>18</sup>F-FDG in dementia in complementarity to MRI findings [7–9]. Future development of new specific tracers will bring additional potential applications of for PET imaging in combination with MRI [10, 11].

---

A.J. Beer (✉) • M. Eiber  
Department of Radiology, Klinikum Rechts der Isar,  
Technische Universität München, Munich, Germany

O. Ratib • J.-P. Willi  
Division of Nuclear Medicine and Molecular Imaging,  
Department of Medical Imaging,  
Geneva University Hospitals,  
Geneva, Switzerland  
e-mail: osman.ratib@hcuge.ch

I. Dregely • M. Essler • S. Foerster • S. Nekolla  
C. Rischpler • I. Yakushev  
Department of Nuclear Medicine,  
Technische Universität München, Munich, Germany

## Atherosclerotic Plaque at Carotid Bifurcation

### Clinical History

Fifty-nine-year-old man with history of an intermittent weakness of the left hand. An ultrasound examination of the right internal carotid artery shows a slight stenosis.

### Imaging Technique

PET/MR image acquired 140 min after iv injection of 421 MBq 18F-FDG.

1 bed position  $\times$  15 min together with axial TOF, T2w TSE, T1w TSE native and post injection of 17 ml of Gd-DTPA MR contrast agent (CA). Head/neck and dedicated phased-array carotid coil.

### Findings

A mild stenosis of right carotid artery slightly above bifurcation is observed. Axial high resolution TSE images show morphology of outward plaque remodeling. Different MR contrast weightings allow distinguishing plaque constituents. Faint uptake of 18F-FDG tracer at plaque location indicates possible inflammatory status of the plaque.

### Teaching Points

In atherosclerosis characterization of the so-called “vulnerable” plaque at risk for disruption is critical to predict adverse events. PET/MR allows for identification of atherosclerotic plaque morphology and functional status.

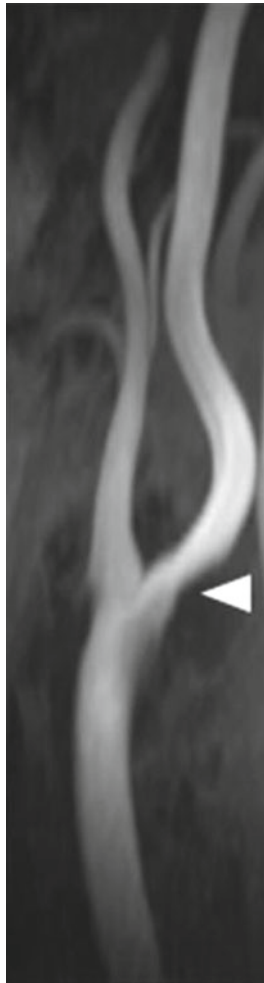


**Fig. 12.1** Slight stenosis observed at carotid artery slightly above bifurcation (*arrowhead*) shown on a MIP projection of axial time-of-flight MR images, acquired without the use of contrast agent

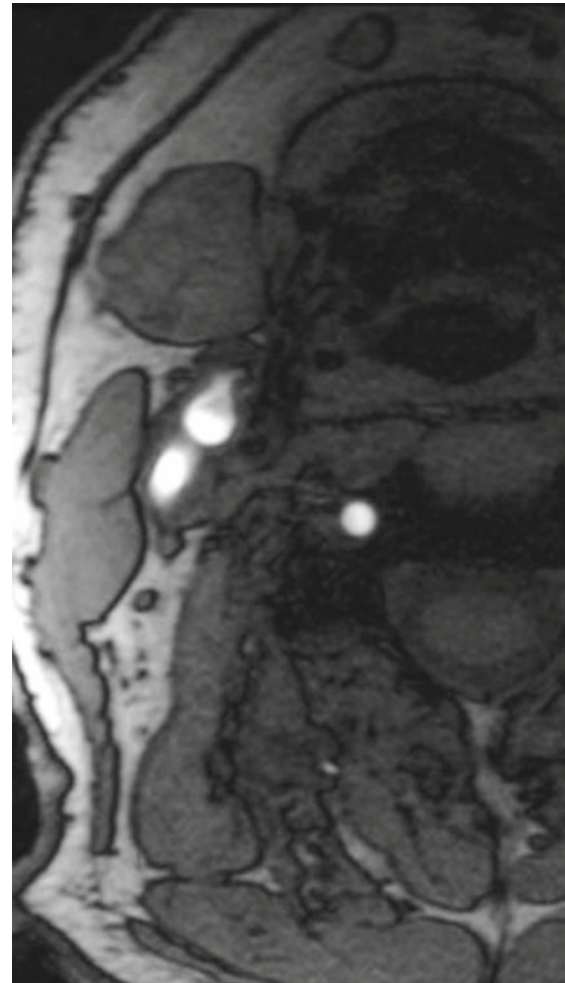


**Fig. 12.2** Axial TOF MR images show slightly restricted lumen due to a plaque, which extends outward to the vessel lumen

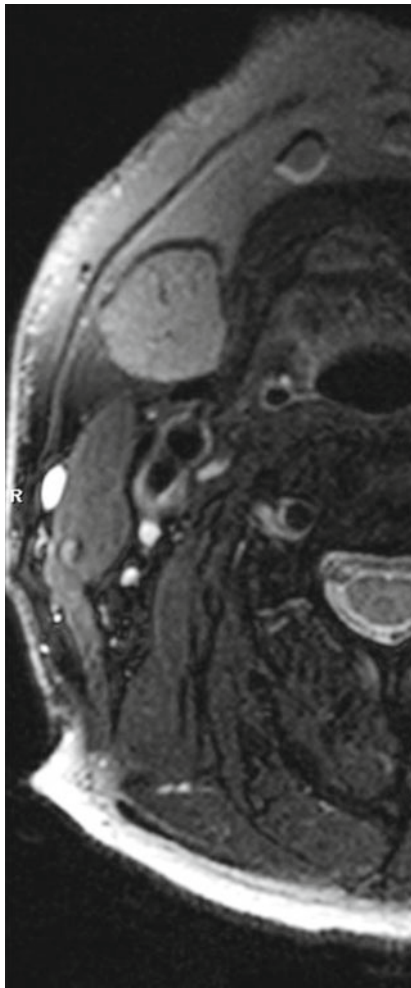


**Fig. 12.3** Bright signal on T2 weighted images show intact fibrous cap as well as additional fibrous constituents in plaque

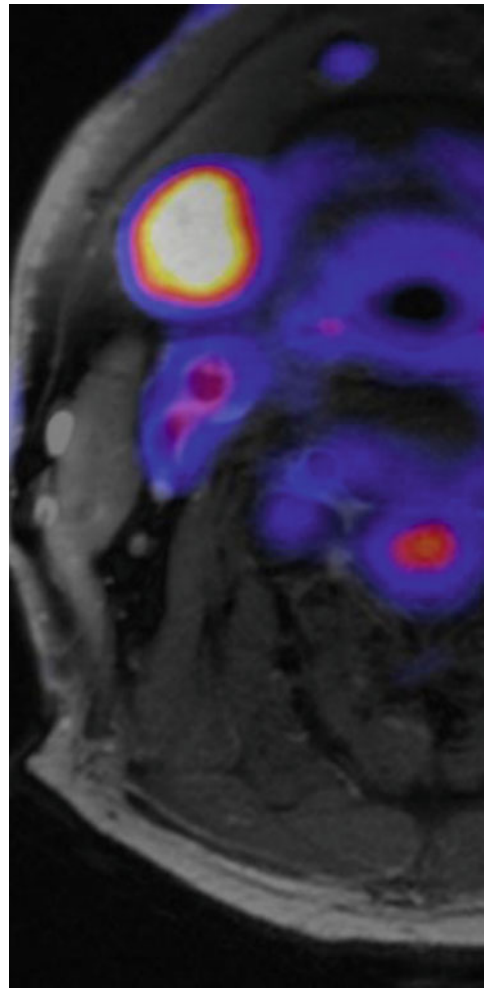


**Fig. 12.5** Fusion of PET and post CA T1w TSE shows a perfect anatomical co-registration of the faint 18F-FDG tracer uptake at the location of the plaque (PET images is calibrated in SUV values, intensity scale 1–3 SUV)

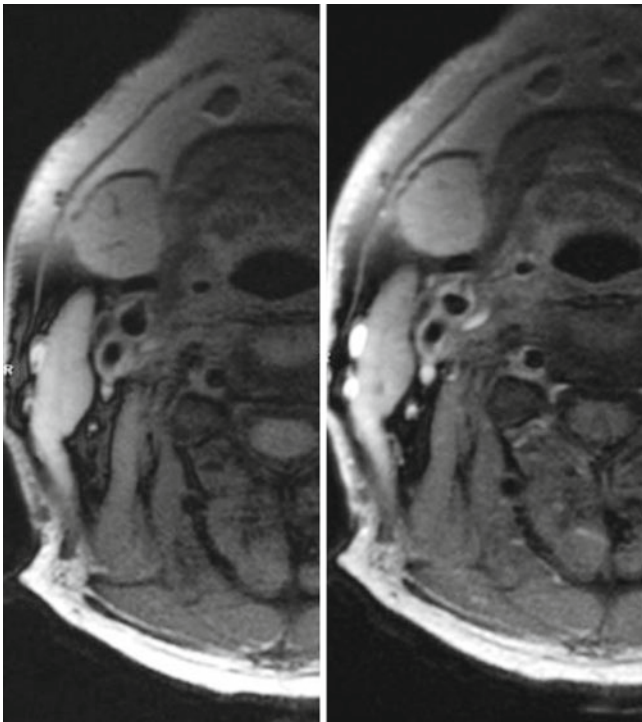


**Fig. 12.4** Lipid is bright on native T1 weighted images (*left image*), if calcium was present it would be dark. Signal enhancement on T1 weighted post CA image (*right image*) indicates fibrous tissue, lipid or calcified areas do not enhance

## Stress Fracture

### Clinical History

Fifty-nine-year-old female patient with osteosynthetic supply of the right ankle after a complex fracture 1.5 years ago. The patient suffers from increasing pain of the right foot developing over the last few months. A prior X-ray was negative.

### Imaging Technique

PET/MR of the right foot acquired 126 min after iv injection 326 MBq <sup>18</sup>F-Fluoride, 78 kg.

1 bed × 10 min together with sagittal T1w TSE/ PDw fs, axial T1w TSE/ PDw fs and coronal T2w TSE. Flex coil.

### Findings

Bone marrow edema and high osteoblastic activity in PET indicate an active process in the cuboid bone. Only mild edema and minor uptake combined with a clear stress fracture line are signs of a more chronic process in the calcaneus.

### Teaching Points

<sup>18</sup>F-Fluoride PET and MRI can provide complementary information in patients with chronic foot pain. The combination of T1w TSE outlining a potential fracture line and the extent of osteoblastic activity is helpful in the differentiation between an active and chronic process.

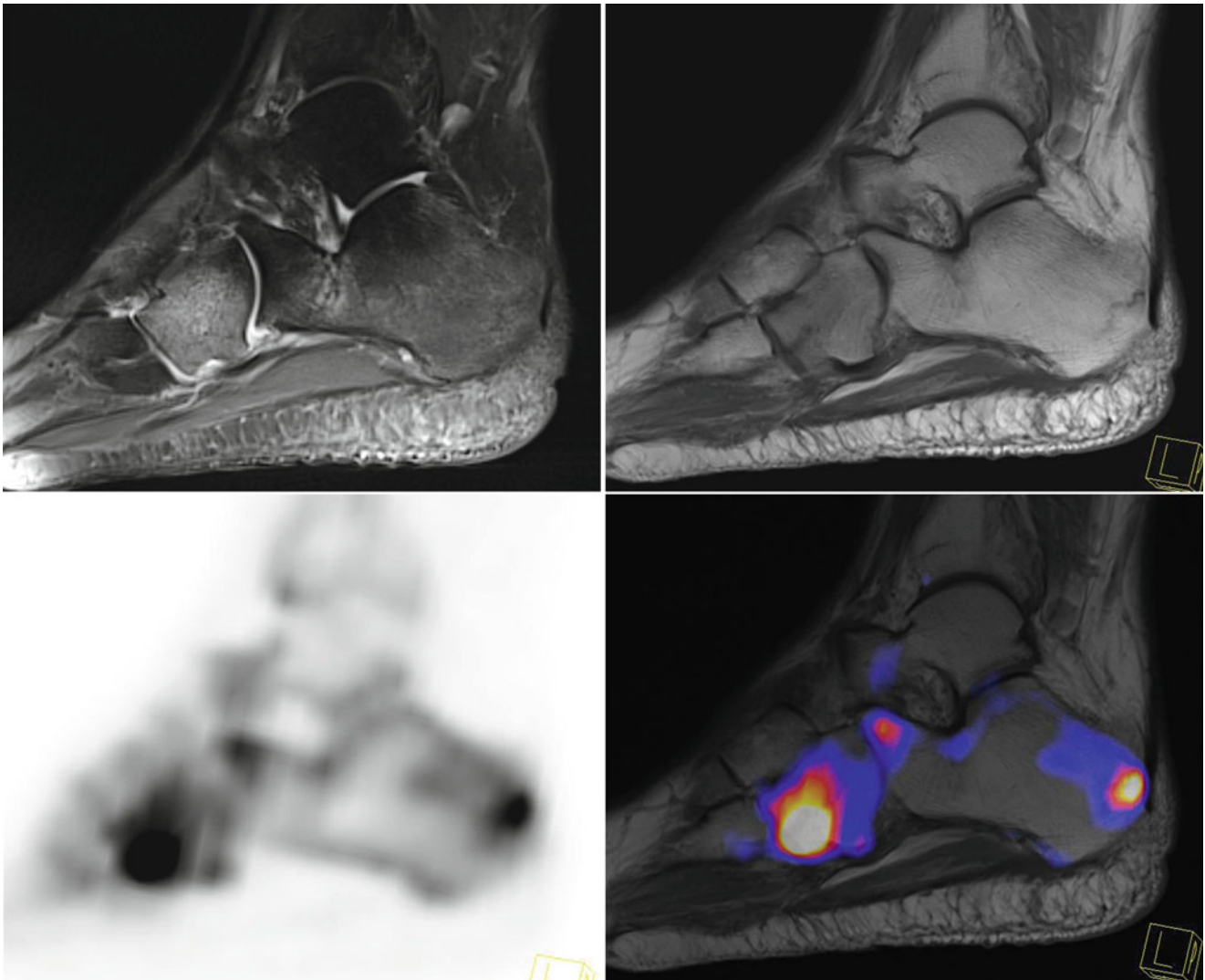


**Fig. 12.6** Sagittal PDw image (*top left*) reveals an extensive hyperintensity in the cuboid bone. Minor bone marrow edema is also found in the dorsal part of the calcaneus. Sagittal T1w TSE shows a hypointense *curved line* in the calcaneus adjacent to the achilles tendon consistent with a stress fracture. In addition a beginning

hypointense line can be found in the anterior part of the cuboid bone (*top right*). An intense uptake of <sup>18</sup>F-Fluoride is found in the cuboid bone indicating high osteoblastic activity. The low and circumscribed uptake in the dorsal part of the calcaneus indicates a more chronic process (*bottom*)

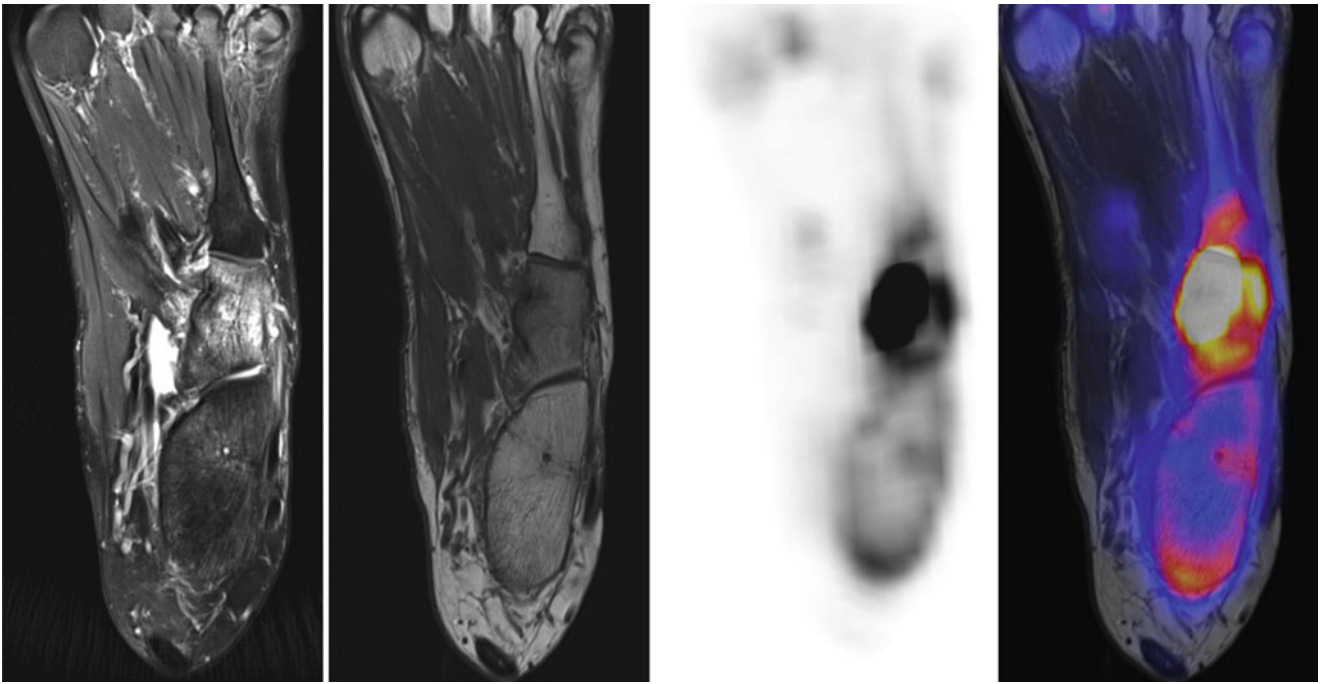


**Fig. 12.7** Axial PDw fs and T1w TSE show an extensive bone marrow edema in the cuboid bone. The beginning fracture line present in the sagittal image is only partially visualized (*left images*).  $^{18}\text{F}$ -Flouride

PET and fused image demonstrate high osteoblastic activity in the cuboid bone (*right images*)



**Fig. 12.8** A prior x-ray of the right ankle is completely normal (*left*). Sagittal reformatted multi-slice computed tomography (MS-CT) shows a curved hyperdense line in the posterior part of the calcaneus

analogous to the findings in T1w TSE (*middle*). The axial reformatted MS-CT cannot outline the beginning fracture line in the cuboid bone (*right*)

## Multicystic Disease

### Clinical History

65 y.o. patient with polycystic disease and status post renal transplant due to renal insufficiency. Diagnostic staging for possible lymphoma.

### Imaging Technique

**PET:** Whole-body PET acquired 60 min after injection of 369 MBq of  $^{18}\text{F}$ -FDG, 57 kg/157 cm patient, with 5.2 mmol/L of fasting glycemia.

**MRI:** Whole body atMR (T1 weighted), supine position. 3D TSE T2 weighted whole-body MRI.

### Findings

PET/MR images confirmed the diffuse polycystic disease with only mild focal uptake of some retro-peritoneal and para-aortic lymph nodes with strong evidence of any malignant disease.

### Teaching Points

In patients with renal insufficiency and complex clinical history, high resolution MR of hybrid PET/MR can replace PET/CT studies for whole-body staging.



**Fig. 12.9** Coronal MIP reconstruction of PET images shows diffuse focal spots of mild FDG uptake in the abdomen

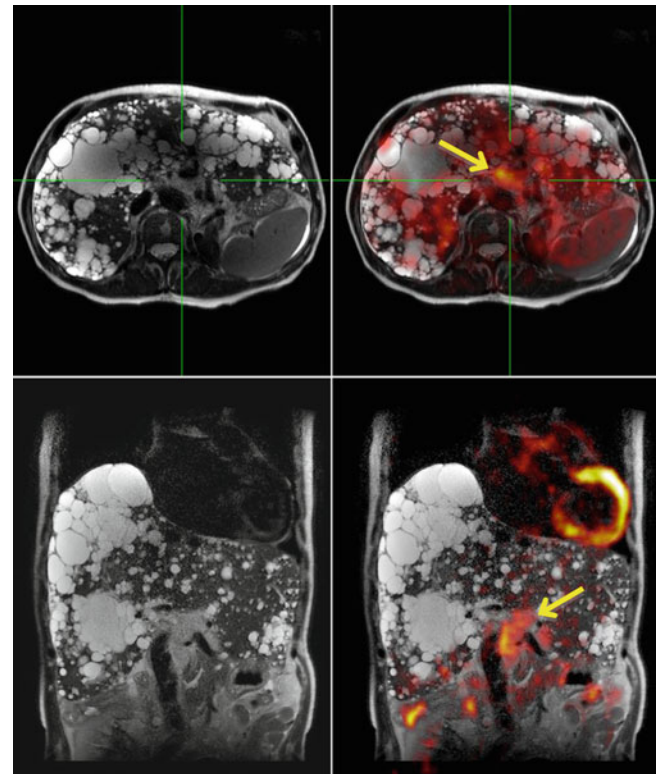


**Fig. 12.10** Axial and coronal respiratory-gated HASTE images (*left*) fused with PET images (*right*), showing mild uptake (*arrow*) of enlarged retro-peritoneal lymph nodes (SUV max 3.2)

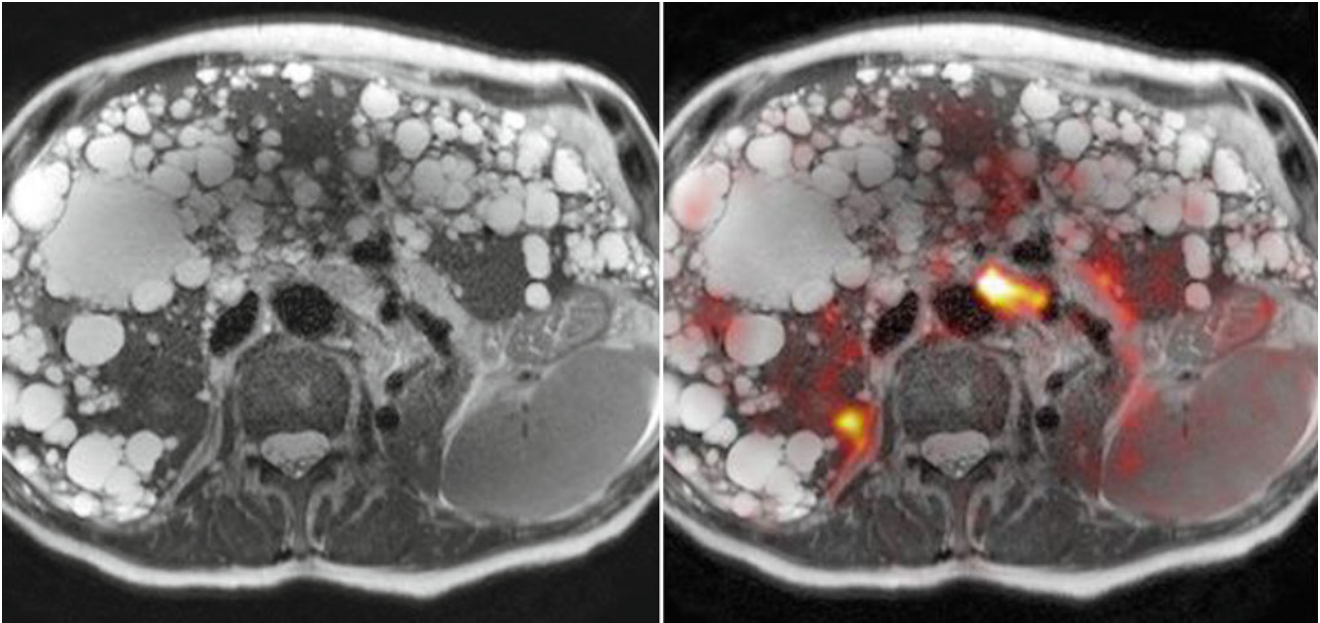


**Fig. 12.11** Axial T2 HASTE MR images showing diffuse polycystic disease fused with PET image showing focal FDG uptake in a para-aortic enlarged lymph-node

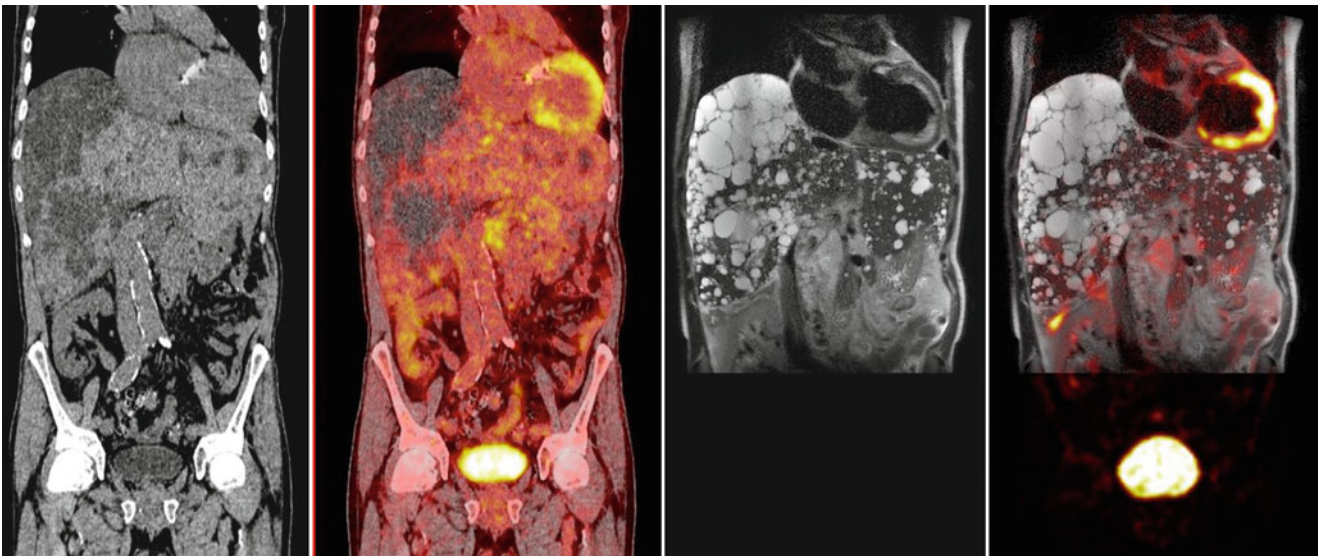


**Fig. 12.12** Comparison of coronal PET/CT (*left*) and high resolution coronal abdominal HASTE images of PET MR study (*right*)

## Kaposi Sarcoma

### Clinical History

61 y.o. patient with known Kaposi sarcoma in an endemic African form associated with HHV8 virus often associated with HIV positive subjects.

### Imaging Technique

**PET:** Whole-body PET acquired 60 min after injection of 377 MBq 18F-FDG, 83 kg/169 cm patient.

**MRI:** Whole body atMR (T1 weighted), supine position. 3D TSE T2 weighted whole-body MRI.



**Fig. 12.13** Coronal MIP reconstruction of PET images shows focal FDG uptake on the right foot (*red arrow*) and single focal lesion of the left thigh (*yellow arrow*)

### Findings

PET/MR images multiple subcutaneous lesions with high FDG uptake corresponding to the Kaposi sarcoma lesions, with only one distant hypermetabolic lesion of the left thigh.

### Teaching Points

In soft-tissue lesions, MRI can provide a wealth of different imaging sequences for better characterization and localization of focal hypermetabolic lesions seen on PET.

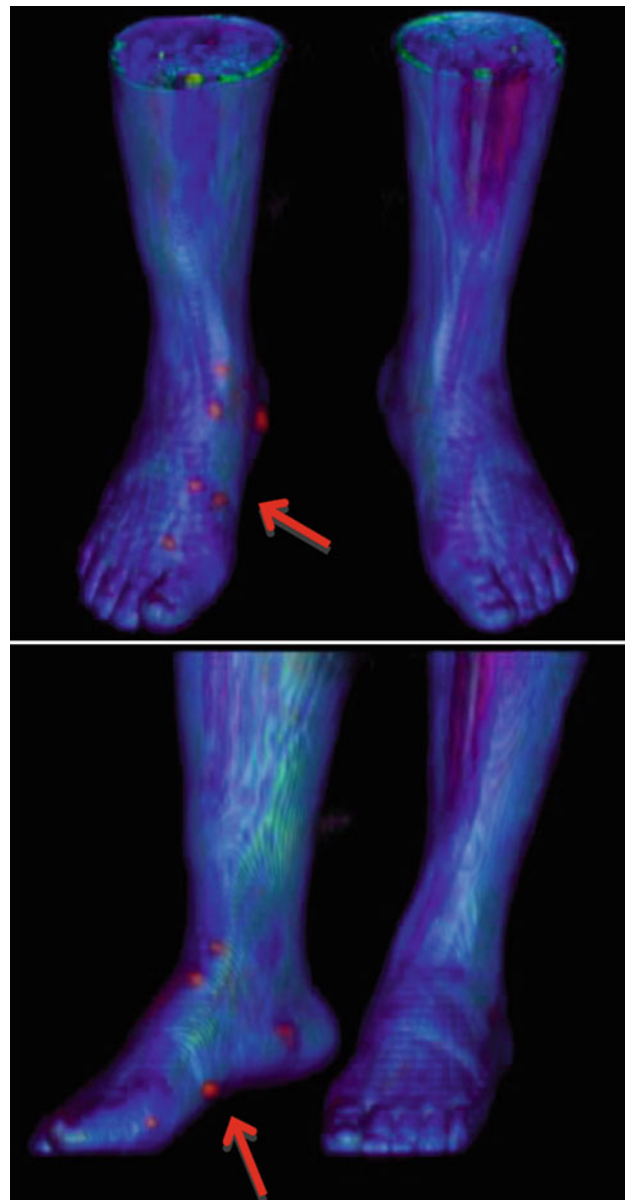


**Fig. 12.14** 3D volume rendering of PET/MR images showing the location of Kaposi lesions on the right foot (*red arrow*)



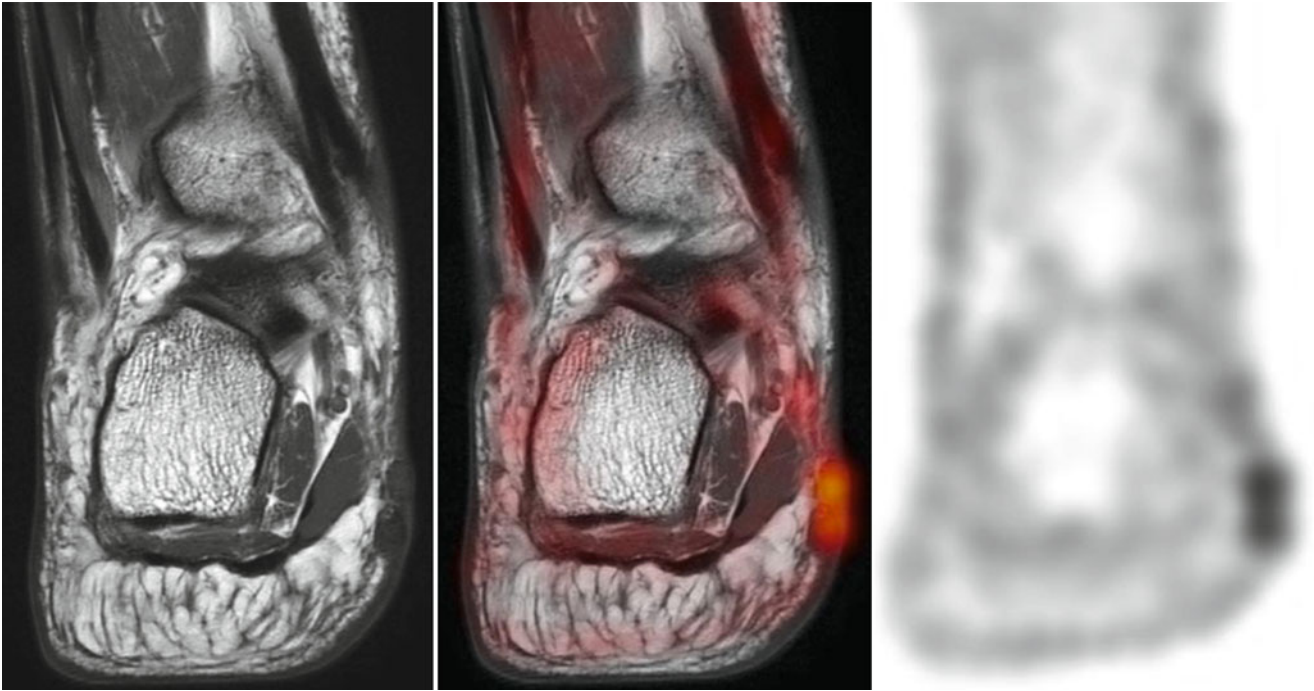


**Fig. 12.15** Coronal high resolution T1 weighted TSE image of the right talus, fused with the corresponding PET image showing two subcutaneous hypermetabolic nodules corresponding to Kaposi sarcoma lesions

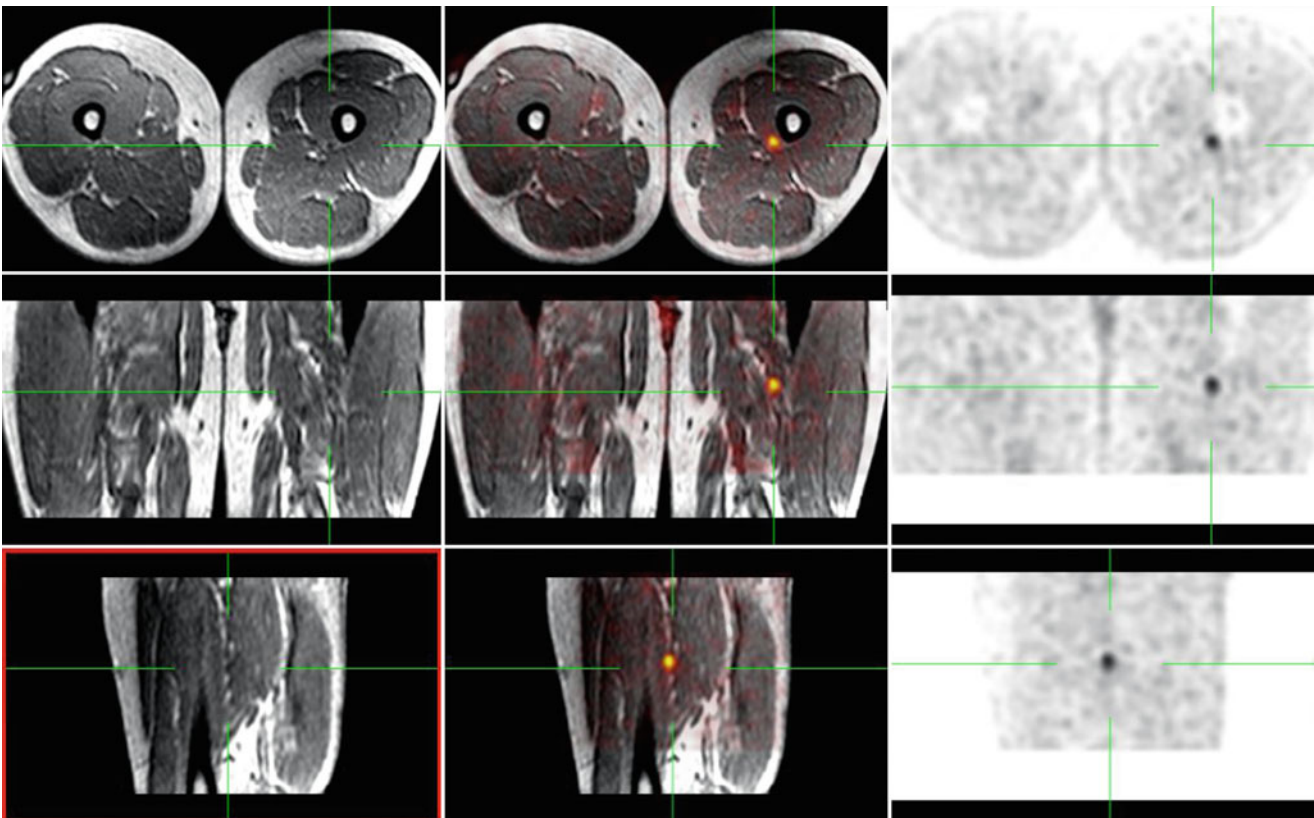


**Fig. 12.16** Multiplaner reformatting (MPR) of T1 weighted TFE PET/MR images showing the focal FDG uptake in the left thigh corresponding to a <10 mm nodule

## Maffucci Syndrome

### Clinical History

29 y.o. patient with a Maffucci syndrome (a rare non-hereditary syndrome characterized by the presence of multiple enchondromas associated with multiple hemangiomas) who underwent several surgical interventions for bone lesions of the lower limbs. Study requested for assessment of a rapidly growing lesion of the left shoulder.

### Imaging Technique

**PET:** Whole-body PET acquired 60 min after injection of 370 MBq of  $^{18}\text{F}$ -FDG.

**MRI:** Whole body atMR (T1 weighted), supine position. 3D TSE T2 weighted whole-body MRI.

### Findings

PET/MR images confirmed the wide spread of enchondroma lesions across the whole body with mild to moderate FDG uptake. A growing lesion of the left shoulder showed moderate homogeneous FDG uptake with no evidence of malignant transformation.

### Teaching Points

Multi-parametric criteria from MRI tissue characteristics and patterns of FDG uptake can help differentiate benign from malignant lesions in soft tissue tumors.



**Fig. 12.17** Coronal MIP reconstruction of PET images shows multiple diffuse lesions with mild to moderate tracer uptake in enchondroma lesions of the limbs

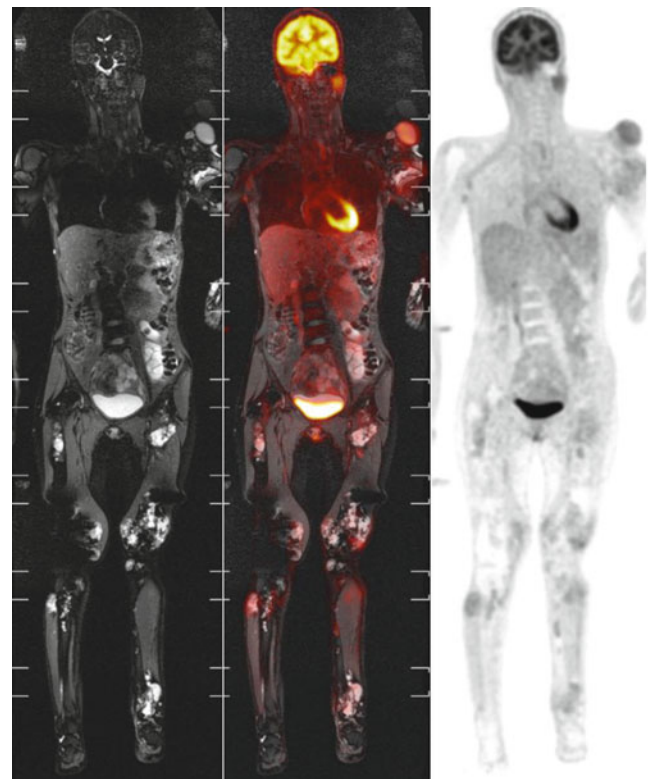


**Fig. 12.18** Coronal STIR MR (*left*) and corresponding whole-body PET image (*right*) with fused images in the middle. Not the important metal artifacts of metal implants in the right knee and left limb

**Fig. 12.19** Comparison of different imaging modalities: (a) conventional X-ray, (b) PET, (c) T1 weighted gadolinium enhanced TSE MRI (d) MR angiogram

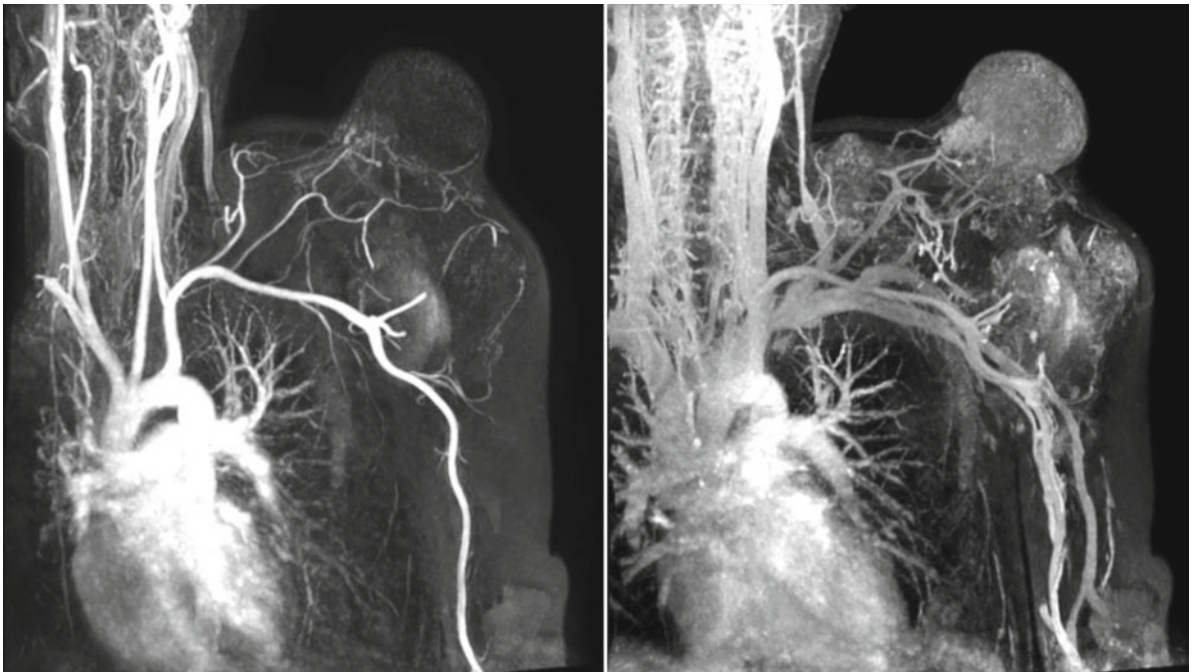
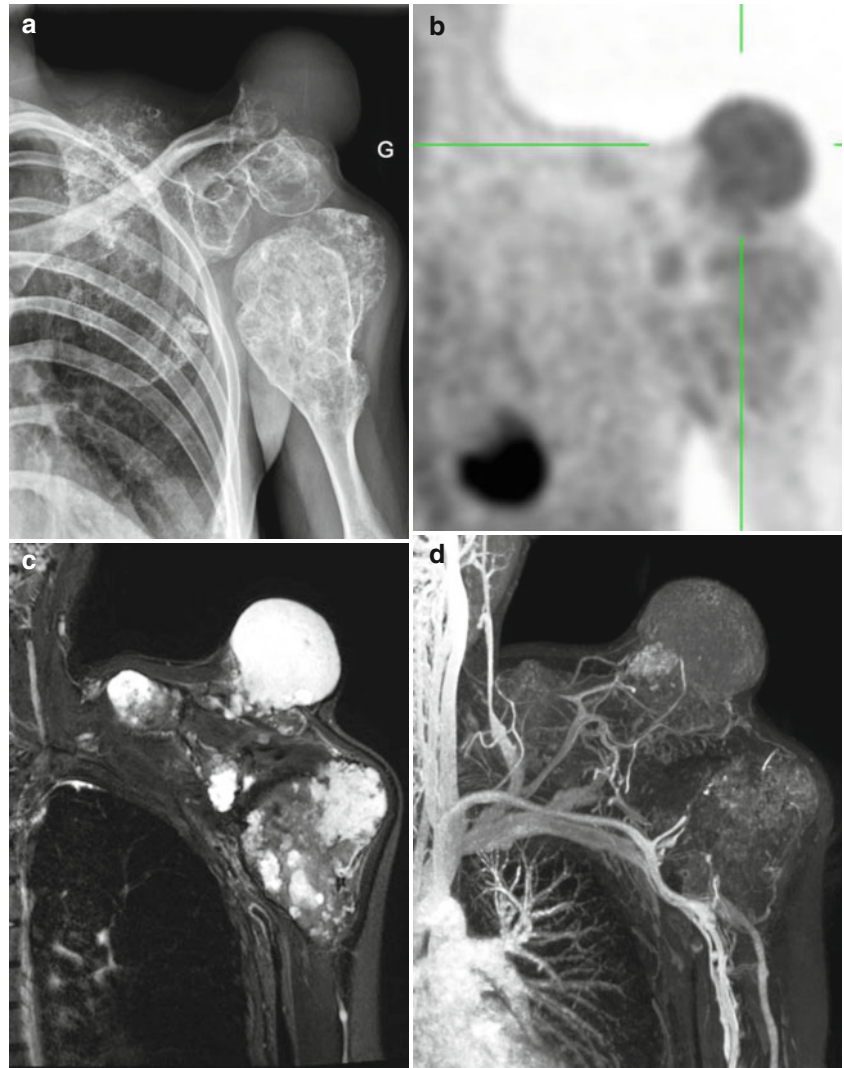


**Fig. 12.20** Arterial (*left*) and venous (*right*) phase of MR angiogram of the left shoulder

## Giant Cell Vasculitis

### Clinical History

Seventy-two-year-old patient presenting with elevated CRP and chest pain.

### Imaging Technique

PET/MR images of the whole body were acquired 108 min after iv injection 420 MBq<sup>18</sup>F-FDG.

Coronal T2w STIR MRI, GRE MRI before and after application of CM.

### Findings

Increased glucose metabolism in the vessel wall of the descending thoracic aorta was found to correlate with hyperintense changes seen in T2w MRI.

### Teaching Points

FDG-PET detects pathological tracer uptake in vascular wall which confirms active vasculitis. MRI helps to localize vascular uptake and allows correlation with morphological changes of the vessel wall.



**Fig. 12.21** FDG-PET shows increased glucose metabolism in the wall of the descending thoracic aorta

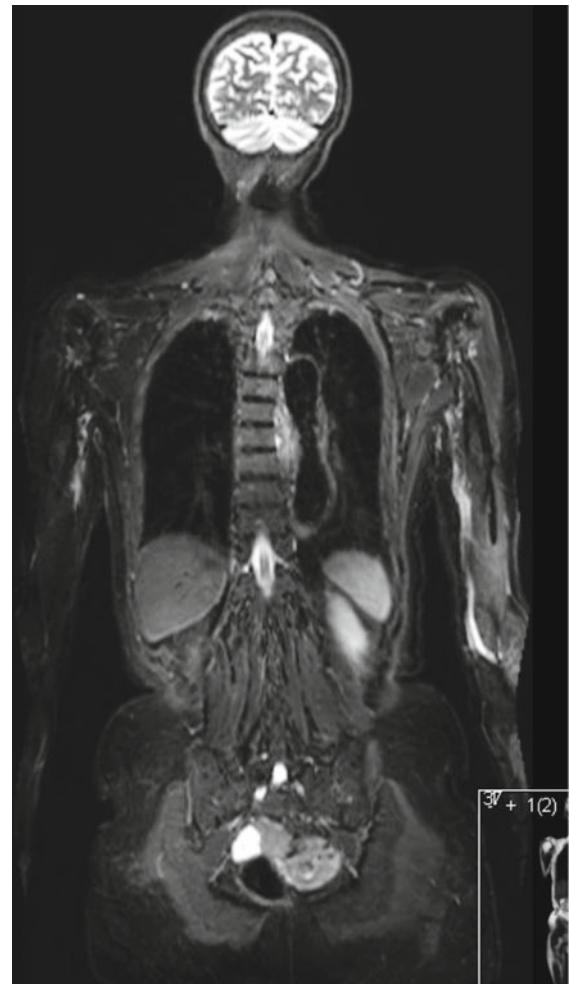


**Fig. 12.22** Coronal T2w STIR MRI shows thickening of the wall of the descending thoracic aorta

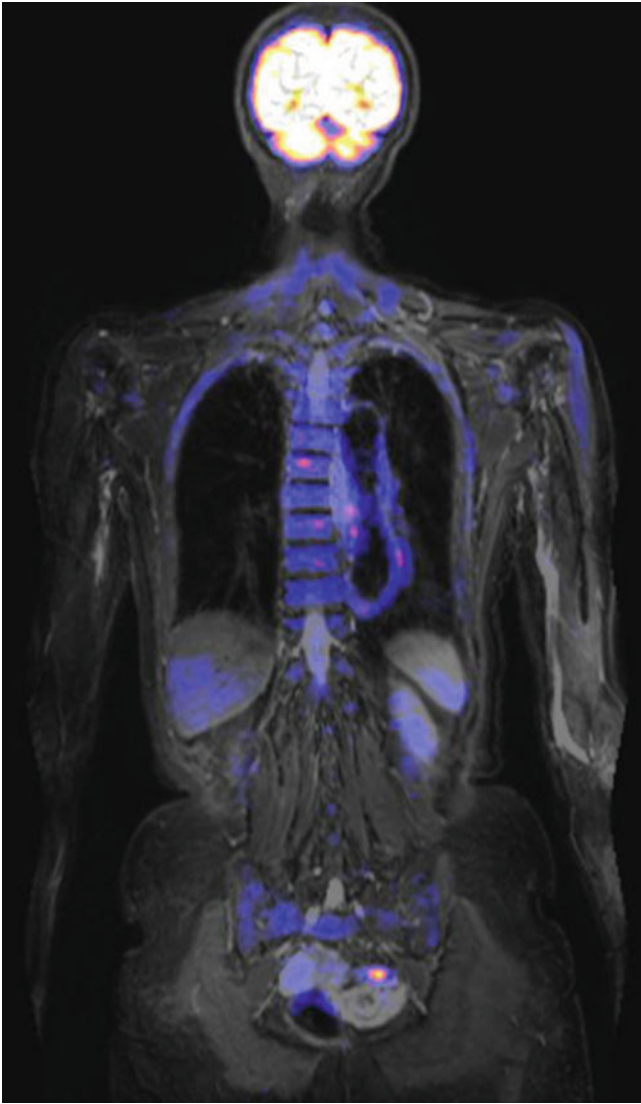


**Fig. 12.23** Colocalization of FDG-uptake and morphological changes are demonstrated by coregistration of MR and PET

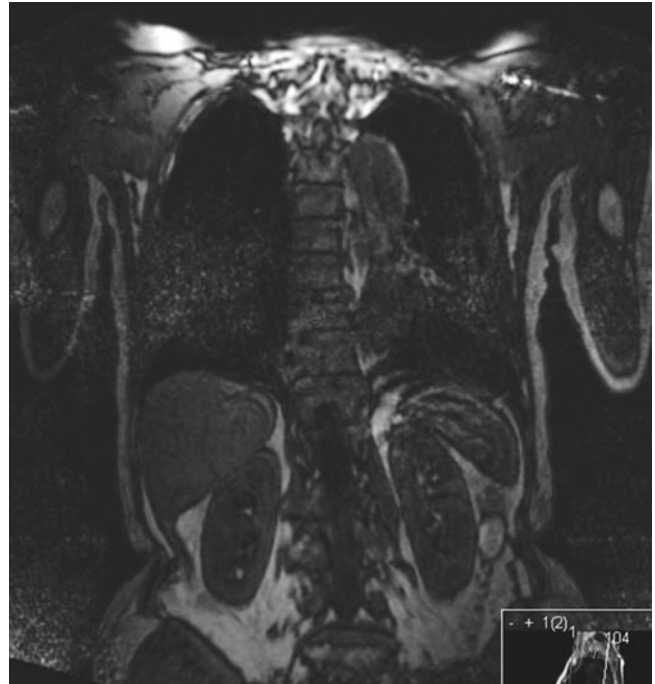


**Fig. 12.24** GRE MRI before injection of contrast media



**Fig. 12.25** GRE MRI after Gadolinium injection shows mild enhancement

## Cardiac Sarcoidosis

### Clinical History

A 30-year-old male patient was referred to our institution because of suspected cardiac involvement of a newly diagnosed sarcoidosis. Coronary angiography excluded coronary artery disease and showed a severely reduced left ventricular function. A CT of the chest demonstrated bihilar lymphadenopathy. Subsequently, the patient was transferred to our institution to confirm cardiac involvement of the sarcoidosis by PET/MR.

### Imaging Technique

To suppress physiological glucose uptake of the myocardium the patient was put on a low-carbohydrate diet for 1 day and had to fast 12 h prior to the scan. PET/MR images were acquired 64 min after iv injection of 238 MBq 18F-FDG.

Furthermore, myocardial perfusion was assessed at resting conditions by slow bolus iv injection over 30 s of 219 MBq  $^{13}\text{N}$ -ammonia. MR: T1 VIBE Dixon for attenuation correction, True-FISP CINE (wall motion), T1 IR 15 min. 40 ml of Gd-DTPA were injected.

### Findings

Bihilar lymphadenopathy with increased FDG uptake in the lymph nodes confirms the diagnosis of sarcoidosis. Areas in the left ventricle with increased FDG uptake and reduced perfusion indicate active inflammation and reveal cardiac involvement of the sarcoidosis. Also, a severely reduced left ventricular ejection fraction with severe hypokinesis of the lateral wall demonstrates dilated cardiomyopathy (DCM) as a consequence of cardiac sarcoidosis. Furthermore, areas demonstrating late gadolinium enhancement (LGE) indicate myocardial infiltration and scarring.

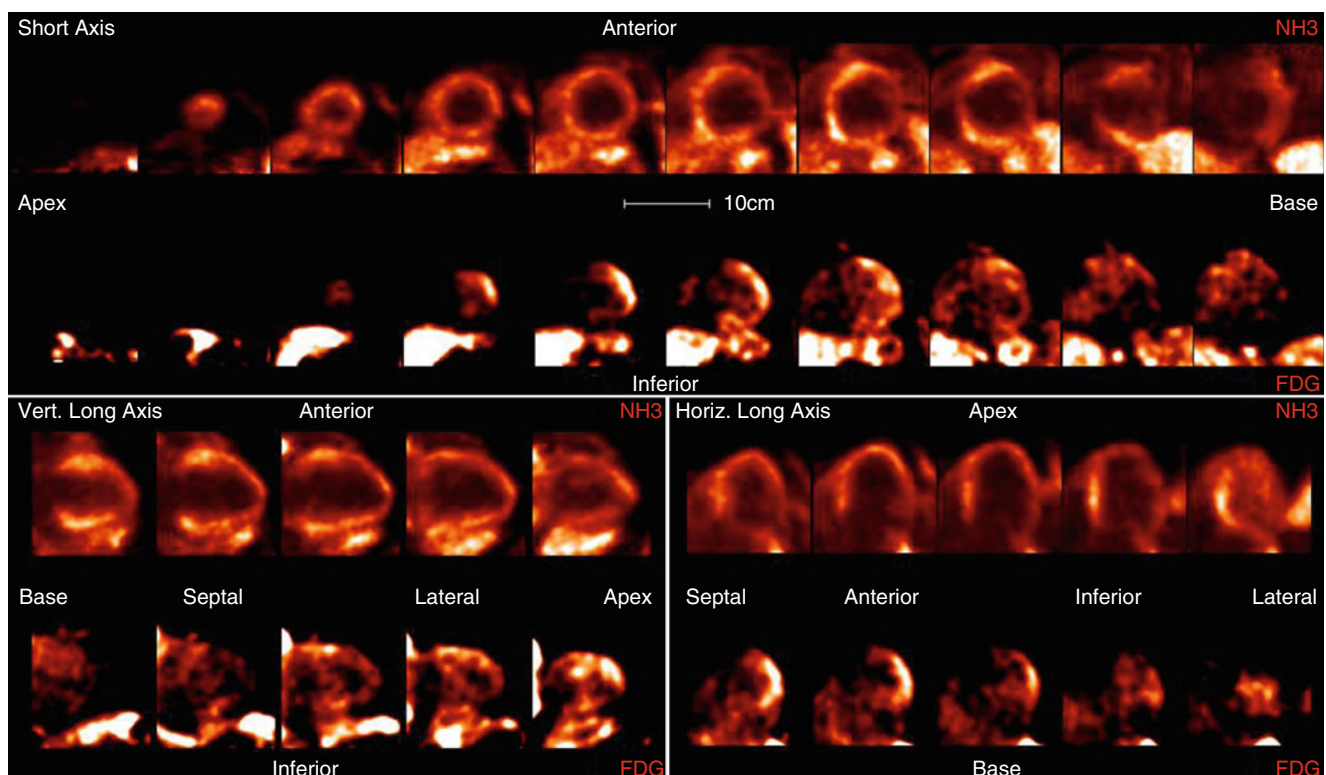


**Fig. 12.26** Illustration of short axis and vertical/horizontal long axis images of the myocardial perfusion (*top rows*) and inflammation (*bottom rows*). Both reduced  $^{13}\text{N}$ -ammonia and upregulated  $^{18}\text{F}$ -FDG

uptake is clearly depicted in the anteriolateral and lateral wall as a sign of active cardiac sarcoidosis in these regions

### Teaching Points

Late gadolinium enhancement appears predominantly in epicardial regions of the myocardium when cardiac involvement of sarcoidosis is present and only rarely spreads to the endocardium. Areas of LGE represent fibrotic changes as a consequence of fibrogranulomatous replacement of the myocardium.

Different patterns of perfusion and glucose metabolism in PET in the case of cardiac involvement of

sarcoidosis are known. Normal perfusion and active inflammation represent an early stage of the disease, while reduced perfusion and active inflammation indicates an advanced stage. Finally, reduced or absent perfusion and no inflammation indicates end-stage cardiac sarcoidosis.

The integrated information of PET and MR allow exact assessment of the stage and inflammatory state of the disease and therapy monitoring.

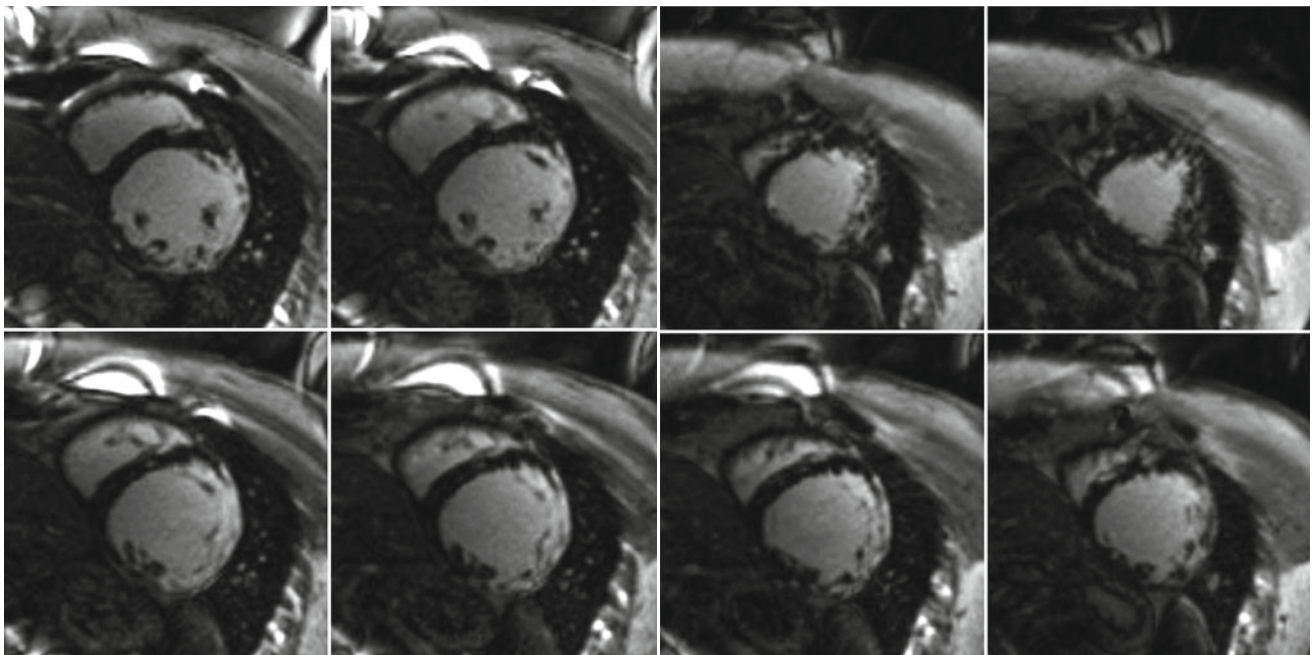


**Fig. 12.27** LGE short axis images of the left ventricle. Large areas of the anterolateral and lateral wall show predominantly epicardial LGE indicating myocardial infiltration and scarring

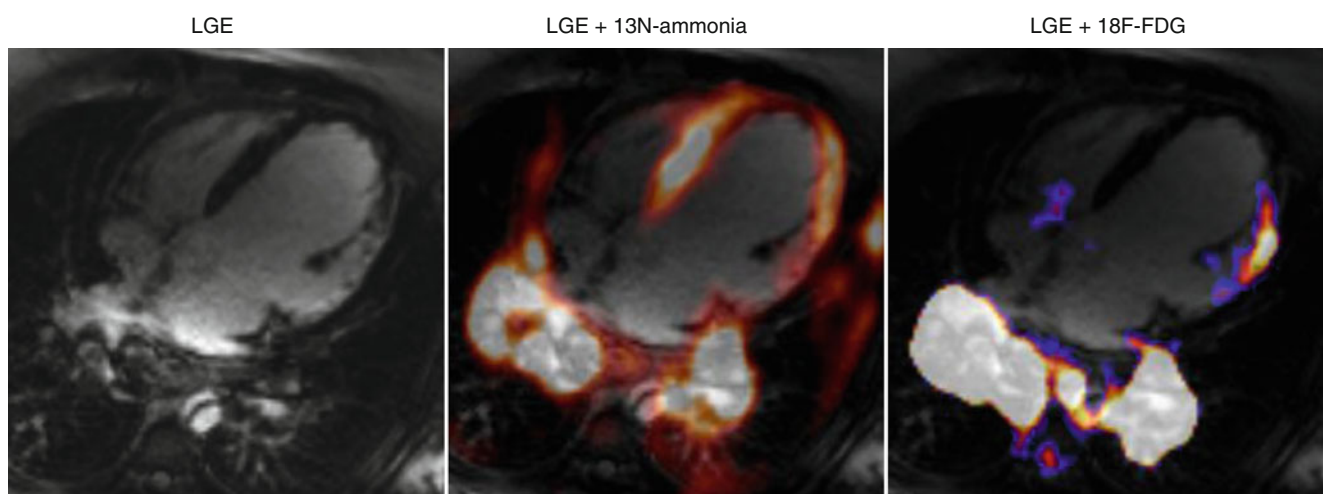


**Fig. 12.28** Four chamber view shows an area of transmural LGE in the lateral wall (*left*). Here clearly reduced perfusion (*middle*) and upregulated glucose metabolism (*right*) is observed as a sign of active

inflammation. Note both increased 13N-ammonia and 18F-FDG uptake in bilateral hilar lymph nodes

## Frontotemporal Dementia (FTD)

### Clinical History

Forty-nine-year-old patient with behavioural deficits and increasing memory loss. Study requested for differential diagnosis of possible neurodegenerative dementia.

### Imaging Technique

PET measurement started 62 min after injection of 151 MBq [18F]FDG. Simultaneous acquisition of MRI sequences (Dixon and 3D T1).

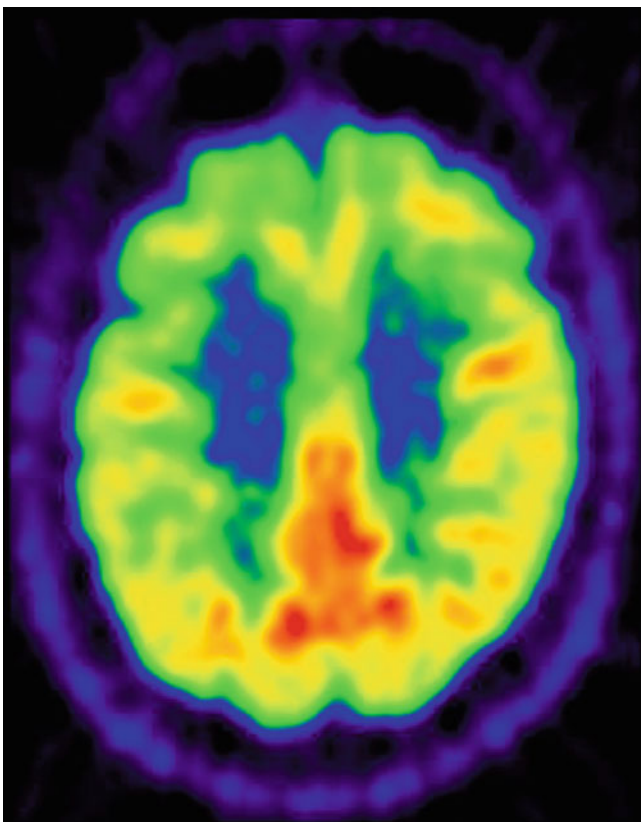


**Fig. 12.29** Patient with frontotemporal dementia (FTD) known as Pick's Disease, a frontal form of fronto-temporal-lobe degenerations. Axial [18F]FDG PET image showing the characteristic regional deficits with reduced bihemispheric [18F]FDG tracer uptake in the frontal lobe and relative sparing of posterior brain regions

### Findings

Transaxial PET image shows a pattern of reduced bihemispheric [18F]FDG tracer uptake in the frontal lobe and relative sparing of posterior brain regions, especially the parietal. The fusion images (Fig. 12.32) [18F]FDG-PET/T1w MRI in 3 projections shows that the regions of reduced [18F]FDG tracer uptake correspond to the regions with most pronounced brain atrophy (frontal lobe). Finally, coronal T1w MRI (below) shows no signs of hippocampal atrophy.

### Teaching Points

The combination of functional [18F]FDG-PET and structural MR information leads to the most likely diagnosis of frontotemporal dementia (FTD). The main differential diagnosis behavioural atypical variant of Alzheimer's Disease (AD) is unlikely due to normal metabolism in the precuneus/posterior cingulate region and due to lack of hippocampal atrophy.

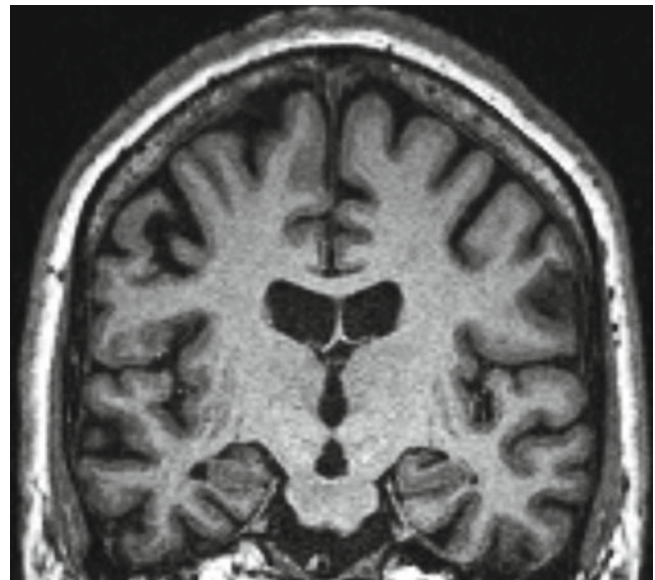


**Fig. 12.30** Coronal T1w MRI showing no signs of hippocampal atrophy



**Fig. 12.31** Multi-planar reformatted PET images show the characteristic regional deficits in FDG uptake in a patient with Pick's Disease with reduced bihemispheric FDG tracer uptake in the frontal lobe and relative sparing of posterior brain regions

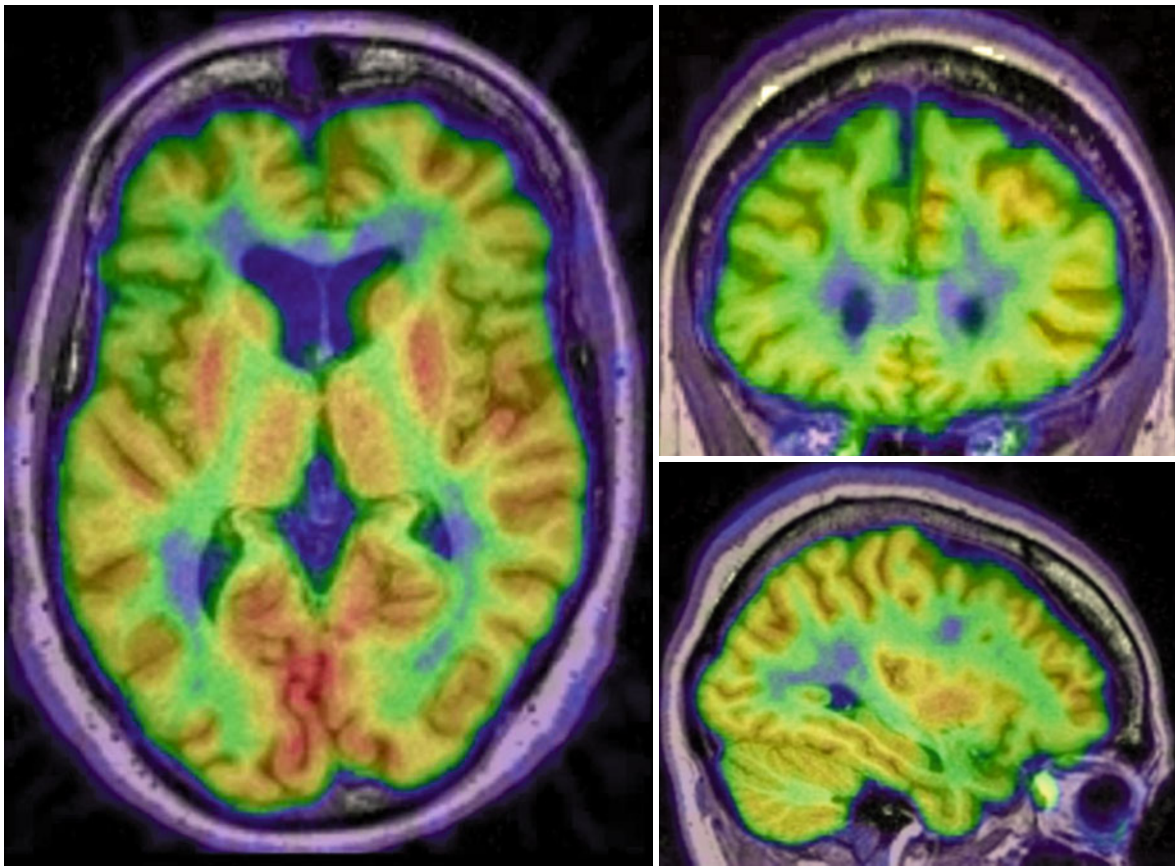
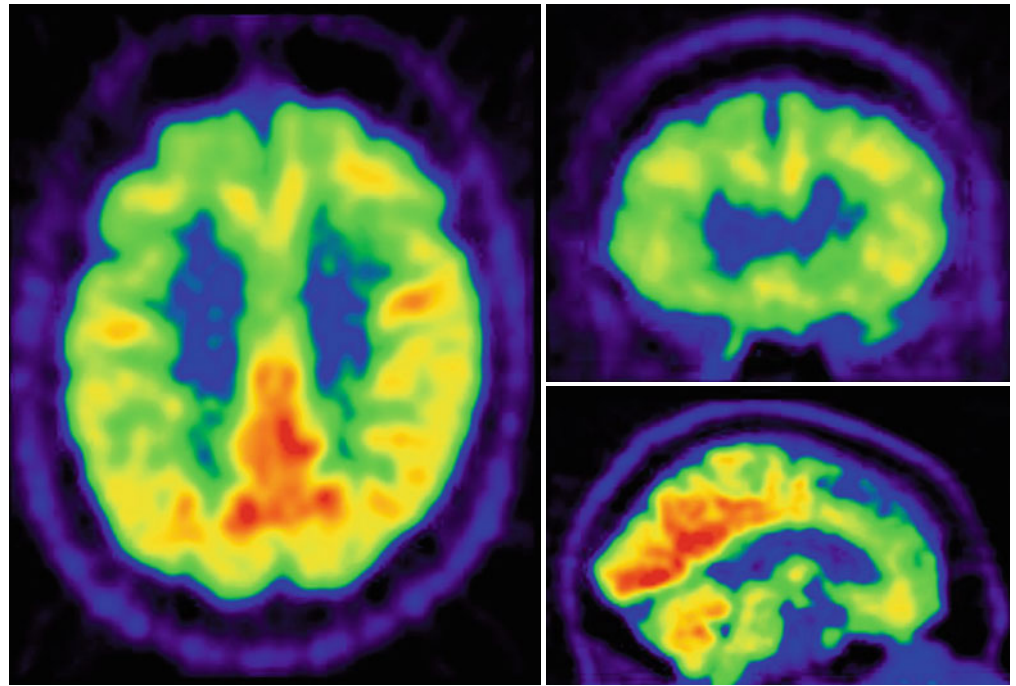


**Fig. 12.32** Fused axial (*left*) coronal (*middle*) and sagittal (*right*) of PET and T1W MRI images showing the characteristic regional deficits in FDG uptake reduction and atrophy

## Alzheimer's Disease (AD)

### Clinical History

Seventy-three-year-old male subject with slowly progressing memory deficits since 4 years. Study requested for differential diagnosis of neurodegenerative dementia.

### Imaging Technique

[18F]FDG-PET measurement started 57 min after injection of 155 MBq [18F]FDG. Simultaneous acquisition of MRI sequences (Dixon, 3D T1 and coronal T2).

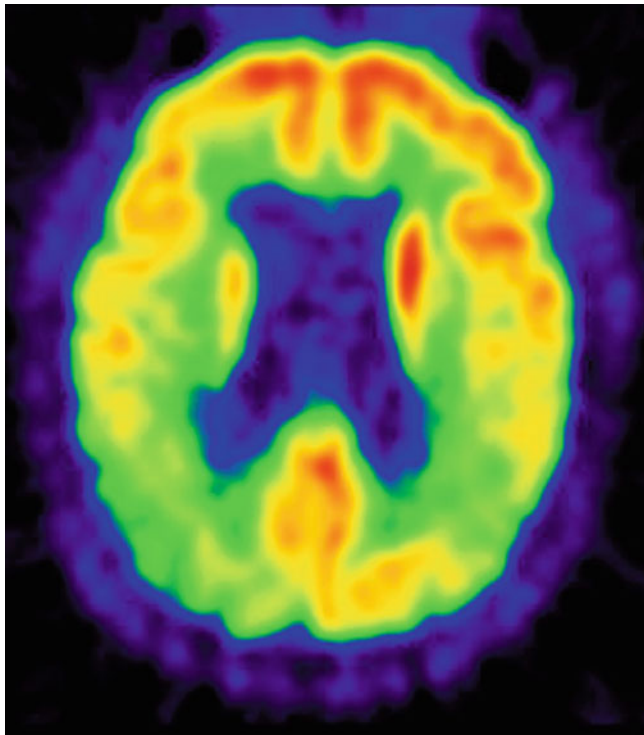


**Fig. 12.33** [18F]FDG-PET in axial projection shows a symmetrically reduced tracer uptake in the bilateral dorsolateral parietal cortex as well as decreased uptake in the right precuneus/posterior cingulate cortex

### Findings

Parietal hypometabolism in [18F]FDG-PET images is indicative of AD. MRI data including volumetric T1w sequence showing severe global brain atrophy as well as hippocampal atrophy in T2 w coronal sequence confirms the diagnosis.

### Teaching Points

The combination of functional and structural information strengthens the diagnosis of Alzheimer's Disease.

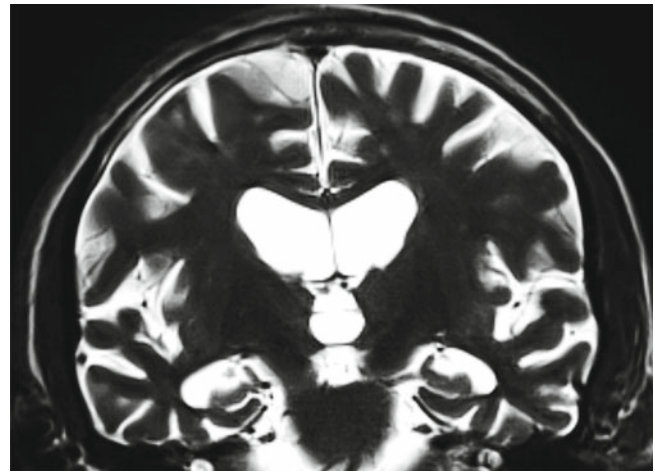


**Fig. 12.34** T2w MRI in coronal orientation demonstrates severe bilateral hippocampal atrophy

**Fig. 12.35** T1w structural MRI in 3 projections shows a parietal-emphasized global atrophy. The image on the *bottom right* demonstrates a fusion with FDG-PET that highlights a spatial overlap between lateral parietal hypometabolism and cortical atrophy

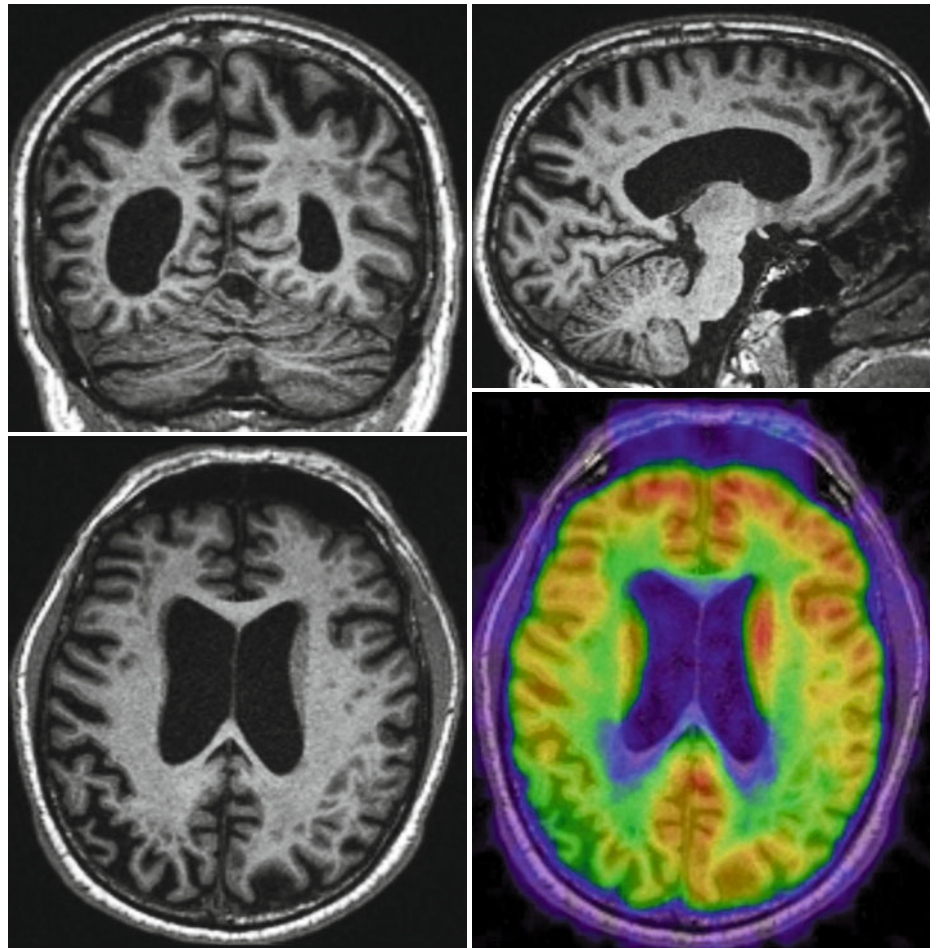
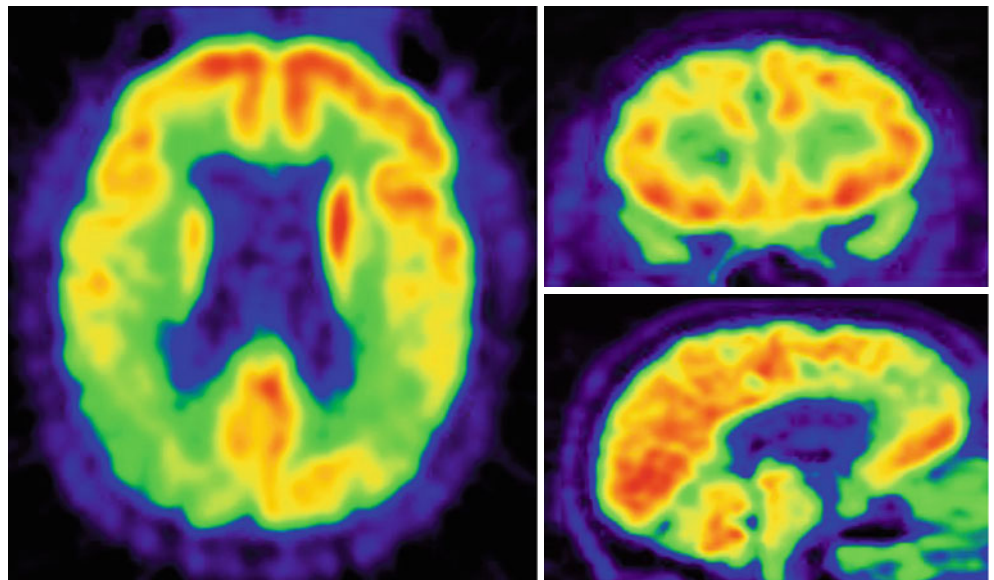


**Fig. 12.36** Multi-planar reformatting (MPR) of FDG-PET images showing a characteristic symmetrically reduced tracer uptake in the bilateral dorsolateral parietal cortex and in the right precuneus/posterior cingulate cortex



## Posterior Cortical Atrophy

### Clinical History

Sixty-eight-year-old patient with predominant visuo-spatial deficits as well as cognitive decline. Neurodegenerative dementia? DD? Structural abnormality?

### Imaging Technique

Two separate studies were performed with different tracers: F18-FDG and C11-PIB. FDG-PET measurement started 60 min after injection of 151 MBq F18-FDG. PiB-PET measurement started 41 min after injection of 371 MBq C11-PiB. Simultaneous acquisition of MRI sequences (Dixon, 3D T1).

### Findings

Transaxial FDG-PET images (Fig. 12.37) show an asymmetrically reduced parietal and temporo-occipital FDG tracer uptake predominantly in the right occipital lobe extending from the cortex into the white matter including a photopenic lesion without any FDG uptake. The fusion images FDG-PET/T1w MRI in 3 projections (Fig. 12.38) show that the photopenic lesion without any FDG tracer uptake corresponds to an irregular dorsal extension of the right ventricle. Additionally, reduced bilateral occipital FDG tracer uptake and the respective occipital cortical atrophy is seen. PiB-PET image (Fig. 12.39) shows diffusely increased PiB tracer uptake in bilateral cortical regions peaking in the precuneus as well as increased subcortical PiB tracer uptake in bilateral striatum.

### Teaching Points

Although information provided by PET alone would already favour diagnosis of AD, structural MR information helps in further differentiating the etiology by clarifying the asymmetrical hypometabolic/photopenic lesion in the right occipital lobe and in detecting the distinct bilateral occipital cortical atrophy, suggesting posterior cortical atrophy as final diagnosis.

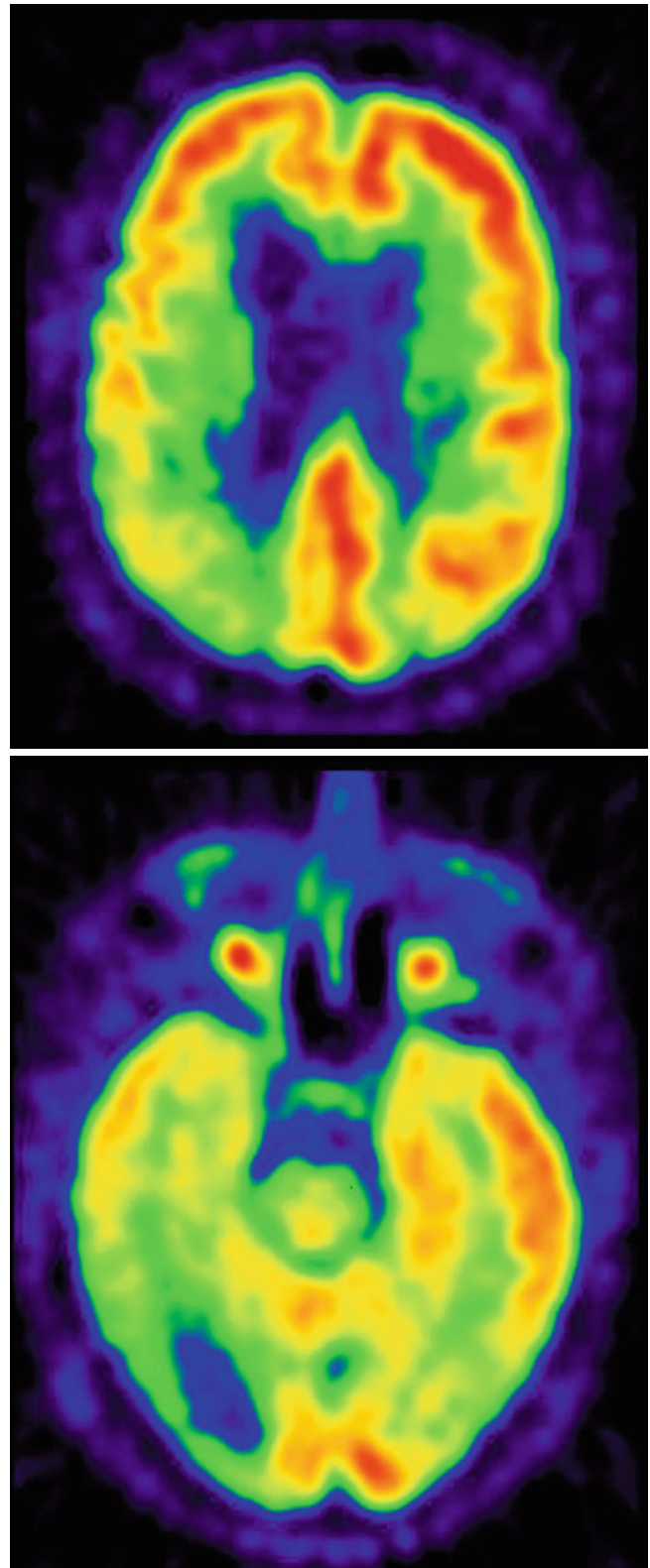


**Fig. 12.37** Two axial PET images showing asymmetrically reduced parietal and temporo-occipital FDG tracer uptake predominantly in the right occipital lobe extending from the cortex into the white matter

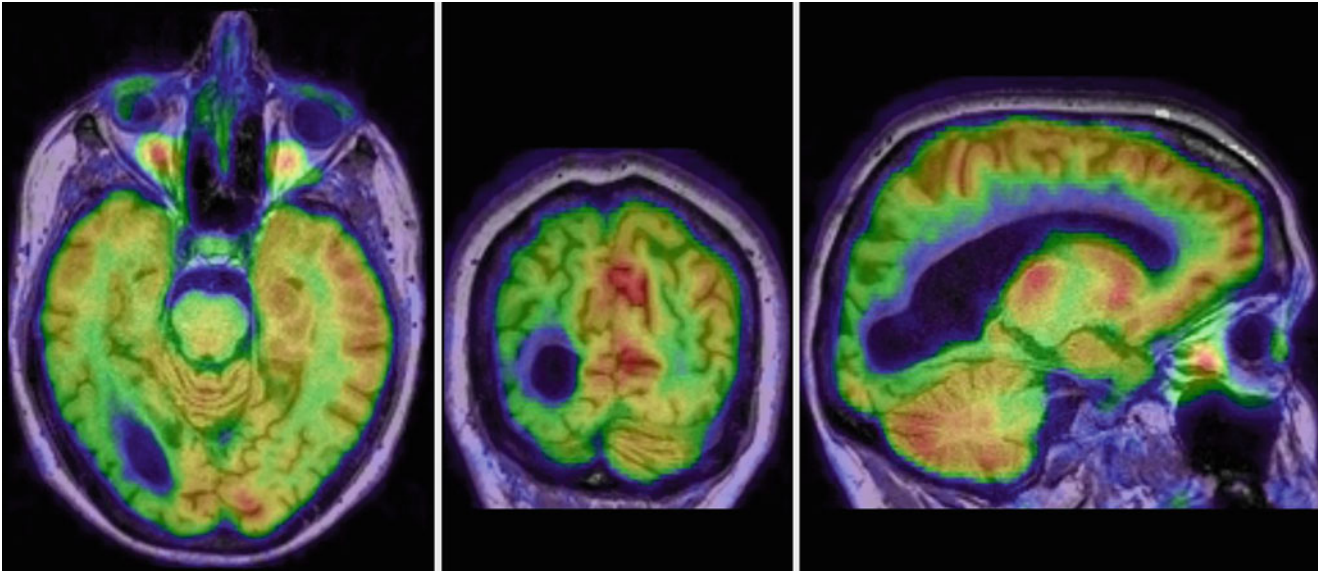


**Fig. 12.38** Multiplanar reformatted (MPR) FDG PET images fused with axial (*left*) coronal (*middle*) and sagittal (*right*) of T1W MRI images show that the photopenic lesion without any FDG tracer uptake

corresponds to an irregular dorsal extension of the right ventricle. Additionally reduced occipital FDG uptake and occipital cortical atrophy can be appreciated

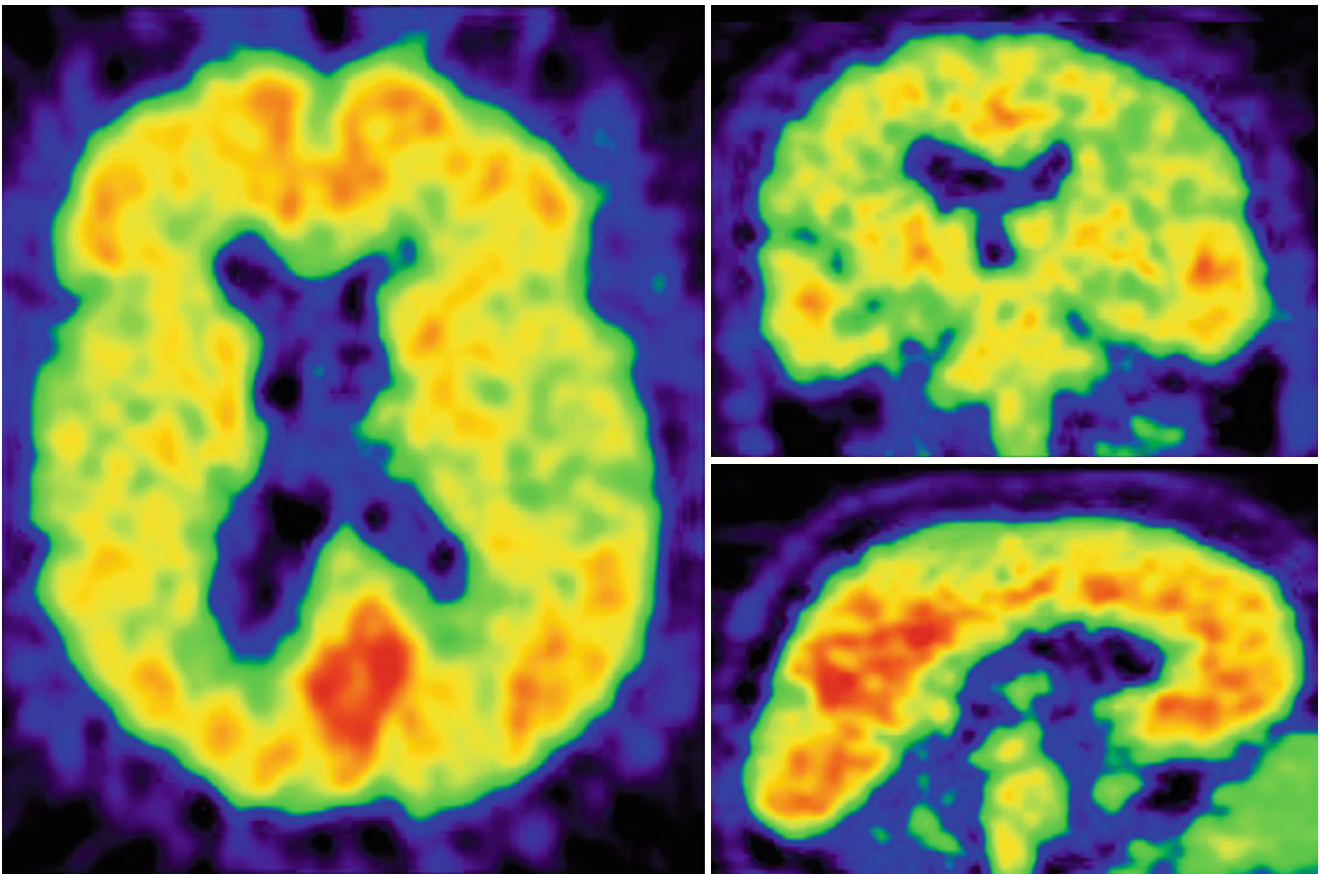


**Fig. 12.39** Multiplanar reformatted images in axial, coronal and sagittal planes of C11-PIB PET images shows diffusely increased PiB tracer uptake in bilateral cortical regions peaking in the precuneus as well as increased subcortical PiB tracer uptake in bilateral striatum

## References

1. Balink H, Collins J, Bruyn GA, Bruyn G, Gemmel F (2009) F-18 FDG PET/CT in the diagnosis of fever of unknown origin. *Clin Nucl Med* 34:862–868
2. Basu S, Kumar R, Alavi A (2010) PET and PET/CT imaging in infection and inflammation: its critical role in assessing complications related to therapeutic interventions in patients with cancer. *Indian J Cancer* 47:371–379
3. Yokota S, Kikuchi M, Nozawa T, Kizawa T, Kanetaka T, Kadota K, Miyamae T, Mori M (2012) Febrile responses in patients with pediatric rheumatic diseases. *Nihon Rinsho Meneki Gakkai Kaishi* 35:511–519
4. Temma T, Saji H (2012) Radiolabelled probes for imaging of atherosclerotic plaques. *Am J Nucl Med Mol Imaging* 2:432–447
5. Dweck MR, Chow MWL, Joshi NV, Williams MC, Jones C, Fletcher AM, Richardson H, White A, McKillop G, van Beek EJR, Boon NA, Rudd JHF, Newby DE (2012) Coronary arterial 18F-sodium fluoride uptake: a novel marker of plaque biology. *J Am Coll Cardiol* 59:1539–1548
6. Hermann S, Starsichova A, Waschkau B, Kuhlmann M, Wenning C, Schober O, Schäfers M (2012) Non-FDG imaging of atherosclerosis: will imaging of MMPs assess plaque vulnerability? *J Nucl Cardiol* 19:609–617
7. Arnaldi D, Morbelli S, Morrone E, Campus C, Nobili F (2012) Cognitive impairment in degenerative parkinsonisms: role of radionuclide brain imaging. *Q J Nucl Med Mol Imaging* 56:55–67
8. de Souza LC, Lehericy S, Dubois B, Stella F, Sarazin M (2012) Neuroimaging in dementias. *Curr Opin Psychiatry* 25:473–479
9. Lopez OL, McDade E, Riverol M, Becker JT (2011) Evolution of the diagnostic criteria for degenerative and cognitive disorders. *Curr Opin Neurol* 24:532–541
10. Heiss W-D, Zimmermann-Meinzingen S (2012) PET imaging in the differential diagnosis of vascular dementia. *J Neurol Sci* 322:268–273
11. Lopez OL, McDade E, Riverol M, Becker JT (2011) Evolution of the diagnostic criteria for degenerative and cognitive disorders. *Curr Opin Neurol* 24:532–541